NASA/TM—20205007760

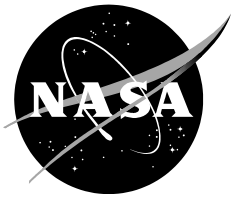

TESS Data Release Notes:
Sector 27, DR38

Michael M. Fausnaugh, Christopher J. Burke
Kavli Institute for Astrophysics and Space Science, Massachusetts Institute of Technology, Cambridge, Massachusetts

Douglas A. Caldwell
SETI Institute, Mountain View, California

Jon M. Jenkins
NASA Ames Research Center, Moffett Field, California

Jeffrey C. Smith, Joseph D. Twicken
SETI Institute, Mountain View, California

Roland Vanderspek
Kavli Institute for Astrophysics and Space Science, Massachusetts Institute of Technology, Cambridge, Massachusetts

John P. Doty
Noqsi Aerospace Ltd, Billerica, Massachusetts

Eric B. Ting
Ames Research Center, Moffett Field, California

Joel S. Villasenor
Kavli Institute for Astrophysics and Space Science, Massachusetts Institute of Technology, Cambridge, Massachusetts

September 16, 2020

NASA STI Program ... in Profile

Since its founding, NASA has been dedicated to the advancement of aeronautics and space science. The NASA scientific and technical information (STI) program plays a key part in helping NASA maintain this important role.
The NASA STI program operates under the auspices of the Agency Chief Information Officer. It collects, organizes, provides for archiving, and disseminates NASA's STI. The NASA STI program provides access to the NTRS Registered and its public interface, the NASA Technical Reports Server, thus providing one of the largest collections of aeronautical and space science STI in the world. Results are published in both non-NASA channels and by NASA in the NASA STI Report Series, which includes the following report types:

- TECHNICAL PUBLICATION. Reports of completed research or a major significant phase of research that present the results of NASA Programs and include extensive data or theoretical analysis. Includes compilations of significant scientific and technical data and information deemed to be of continuing reference value. NASA counterpart of peer-reviewed formal professional papers but has less stringent limitations on manuscript length and extent of graphic presentations.

- TECHNICAL MEMORANDUM.
  Scientific and technical findings that are preliminary or of specialized interest, e.g., quick release reports, working papers, and bibliographies that contain minimal annotation. Does not contain extensive analysis.

- CONTRACTOR REPORT. Scientific and technical findings by NASA-sponsored contractors and grantees.

- CONFERENCE PUBLICATION.
  Collected papers from scientific and technical conferences, symposia, seminars, or other meetings sponsored or co-sponsored by NASA.

- SPECIAL PUBLICATION.
  Scientific, technical, or historical information from NASA programs, projects, and missions, often concerned with subjects having substantial public interest.

- TECHNICAL TRANSLATION.
  English-language translations of foreign scientific and technical material pertinent to NASA's mission.

Specialized services also include organizing and publishing research results, distributing specialized research announcements and feeds, providing information desk and personal search support, and enabling data exchange services.

For more information about the NASA STI program, see the following:

- Access the NASA STI program home page at http://www.sti.nasa.gov

- E-mail your question to help@sti.nasa.gov

- Phone the NASA STI Information Desk at 757-864-9658

- Write to:
  NASA STI Information Desk
  Mail Stop 148
  NASA Langley Research Center
  Hampton, VA 23681-2199

NASA/TM—20205007760

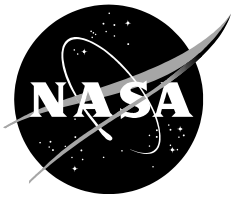

TESS Data Release Notes:
Sector 27, DR38

Michael M. Fausnaugh, Christopher J. Burke
Kavli Institute for Astrophysics and Space Science, Massachusetts Institute of Technology, Cambridge, Massachusetts

Douglas A. Caldwell
SETI Institute, Mountain View, California

Jon M. Jenkins
NASA Ames Research Center, Moffett Field, California

Jeffrey C. Smith, Joseph D. Twicken
SETI Institute, Mountain View, California

Roland Vanderspek
Kavli Institute for Astrophysics and Space Science, Massachusetts Institute of Technology, Cambridge, Massachusetts

John P. Doty
Noqsi Aerospace Ltd, Billerica, Massachusetts

Eric B. Ting
Ames Research Center, Moffett Field, California

Joel S. Villasenor
Kavli Institute for Astrophysics and Space Science, Massachusetts Institute of Technology, Cambridge, Massachusetts

September 16, 2020

Acknowledgements

These Data Release Notes provide information on the processing and export of data from the Transiting Exoplanet Survey Satellite (TESS). The data products included in this data release are full frame images (FFIs), target pixel files, light curve files, collateral pixel files, cotrending basis vectors (CBVs), and Data Validation (DV) reports, time series, and associated xml files.

These data products were generated by the TESS Science Processing Operations Center (SPOC, Jenkins et al., 2016) at NASA Ames Research Center from data collected by the TESS instrument, which is managed by the TESS Payload Operations Center (POC) at Massachusetts Institute of Technology (MIT). The format and content of these data products are documented in the Science Data Products Description Document (SDPDD)[1]. The SPOC science algorithms are based heavily on those of the Kepler Mission science pipeline, and are described in the Kepler Data Processing Handbook (Jenkins, 2020).[2] The Data Validation algorithms are documented in Twicken et al. (2018) and Li et al. (2019). The TESS Instrument Handbook (Vanderspek et al., 2018) contains more information about the TESS instrument design, detector layout, data properties, and mission operations.

The TESS Mission is funded by NASA's Science Mission Directorate.

This report is available in electronic form at
https://archive.stsci.edu/tess/

[1] https://archive.stsci.edu/files/live/sites/mast/files/home/missions-and-data/active-missions/tess/_documents/EXP-TESS-ARC-ICD-TM-0014-Rev-F.pdf

[2] https://archive.stsci.edu/kepler/manuals/KSCI-19081-003-KDPH.pdf

1 Observations

TESS Sector 27 observations include physical orbits 61 and 62 of the spacecraft around the Earth. Data collection was paused for 1.02 days between the orbits to download data. In total, there are 23.35 days of science data collected in Sector 27.

Table 1: Sector 27 Observation times

	UTC	TJD[a]	Cadence #
Orbit 61 start	2020-07-05 18:31:16	2036.27320	582349
Orbit 61 end	2020-07-17 15:01:15	2048.12737	590884
Orbit 62 start	2020-07-18 15:31:15	2049.14820	591619
Orbit 62 end	2020-07-30 03:21:15	2060.64125	599894

[a] TJD = TESS JD = JD - 2,457,000.0

The spacecraft was pointing at RA (J2000): 326.8525°; Dec (J2000): −72.4265°; Roll: 214.5061°. See the TESS project Sector 27 observation page[3] for the coordinates of the spacecraft pointing and center field-of-view of each camera. Fields-of-view for each camera can be found at the TESS Guest Investigator Office observations status page[4].

1.1 New Data Modes

DR38 is the first data release of the TESS extended mission, which introduces a new data mode and shortens the FFI data collection interval.

- Full Frame Images (FFIs) are collected every 10 minutes rather than every 30 minutes, and consist of 240 co-adds of 2-second exposures.
- Select pixel stamps are collected at 20-second cadence, and consist of 10 co-adds of 2-second exposures.

As in the primary mission, select pixel stamps were also collected at 2-minute cadence, consisting of 48 co-adds of 2-second exposures.

Data products associated with the FFIs and 2-minute data products are named in a way consistent with the primary mission data products. Data products for the 20-second mode have the keyword "fast" in the file names; see the SDPDD for full details. For 20-second data, only target pixel files, light curve files, collateral pixel files, and cotrending basis vectors (CBVs) were produced.

Cosmic rays were mitigated in the 2-minute cadence data and 10-minute FFIs by an algorithm running on the instrument firmware. The algorithm examines each pixel in groups of ten consecutive exposures, rejecting the highest and lowest values and summing the rest, resulting in a 20% reduction in the effective exposure time of each cadence (details can be found in Vanderspek et al. 2018). However, the on-board cosmic ray mitigation algorithm

[3] https://tess.mit.edu/observations/sector-27

[4] https://heasarc.gsfc.nasa.gov/docs/tess/status.html

cannot be applied to 20-second data. Instead, cosmic rays were identified and corrected in SPOC data processing. A description of the method is presented in §4.1.

The cadence number (`CADENCENO`) of the 20-second data is an incrementing number chosen so that it does not overlap with the 2-minute cadence number. The `FFIINDEX` number for the 10-minute FFIs is also offset so that it does not overlap with 30-minute `FFIINDEX` numbers from the primary mission.

For the 20-second cadence data, 1,000 targets were selected, which include engineering targets, Guest Investigator targets, and Director Discretionary Time targets. For the 2-minute cadence data, 20,000 targets were selected from engineering targets, a list of bright stars (Tmag < 6), Guest Investigator targets, and Director Discretionary Time targets. The mission also selected 1,500 targets for 2-minute observations, which includes TESS Objects of Interest (TOIs) discovered from Year 1 of the primary mission and promising targets for planet searches based on Year 1 observations. All 20-second targets were also observed at 2-minute cadence.

The detailed target list for both 2-minute and 20-second data, as well as the Guest Investigator target lists, can be found at the Sector 27 observation page[5] and the observations status page[6].

1.2 Notes on Individual Targets

There are no issues with missing light curves or clipped apertures in the 20-second data products.

For the 2-minute cadence data, three bright stars (Tmag $\lesssim 1.8$) with large pixel stamps were not processed in the photometric pipeline. Target pixel files with original and calibrated pixel data are provided,[7] but no light curves were produced. The affected TIC IDs are 238196512, 394046358, 38877693.

Six target stars (167602316, 267211065, 300015238, 730543928, 766018849, 1991380115) are blended with comparably bright stars—the contaminating flux for these objects is very large, and the resulting photometry for such targets is expected to be unreliable.

One target star (2025820827) is closely blended (within 0.5 arcseconds) with a brighter star (392772420). In this case, the assigned aperture is disjoint and the resulting photometry is unreliable.

1.3 Spacecraft Pointing and Momentum dumps

Sector 27 is the first set of observations of the TESS extended mission. Year 3 is a reobservation of the southern ecliptic hemisphere, which will take place over 13 sectors. The pointing strategy is the same as for Year 1, except the locations of Sectors 27–39 are offset in ecliptic longitude with respect to Sectors 1–13. All sectors in Year 3 are planned for a spacecraft pointing of -54 degrees in ecliptic latitude.

[5] https://tess.mit.edu/observations/sector-27

[6] https://heasarc.gsfc.nasa.gov/docs/tess/status.html

[7] Note that the TPF files do not include a background correction for stars without light curves.

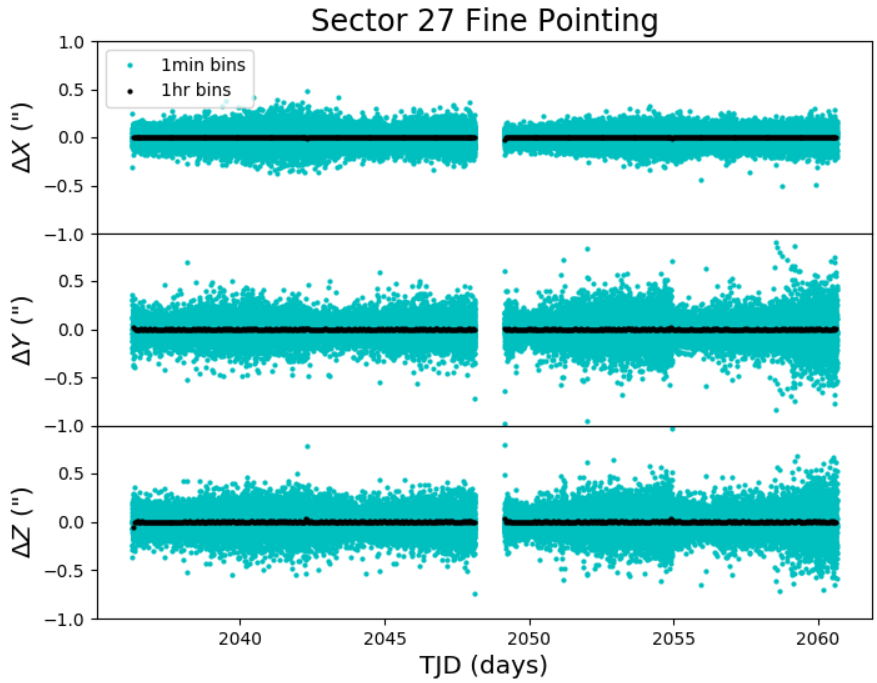

Figure 1: The delta-quaternions from each camera have been converted to spacecraft frame, binned to 1 minute and 1 hour, and averaged across cameras. Long-term trends (such as those caused by differential velocity aberration) have also been removed. The ΔX/ΔY directions represent offsets along the the detectors' rows/columns, while the ΔZ direction represents spacecraft roll.

Camera 1 and Camera 4 were both used for guiding in orbit 61 and orbit 62. A single momentum dump was performed halfway through each orbit. Figure 1 summarizes the pointing performance over the course of the sector based on Fine Pointing telemetry.

1.4 Scattered Light

Figure 2 shows the median value of the background estimate for all targets on a given CCD as a function of time. Figure 3 shows the angle between each camera's boresight and the Earth or Moon—this figure can be used to identify periods affected by scattered light and the relative contributions of the Earth and Moon to the image backgrounds.

In Sector 27, the Earth is a significant source of scattered light throughout both orbits.

2 Data Anomaly Flags

See the SDPDD (§9) for a list of data quality flags and the associated binary values used for TESS data, and the TESS Instrument Handbook for a more detailed description of each flag.

The following flags were not used in Sector 27: bits 1, 2, and 9 (Attitude Tweak, Safe Mode, and Discontinuity).

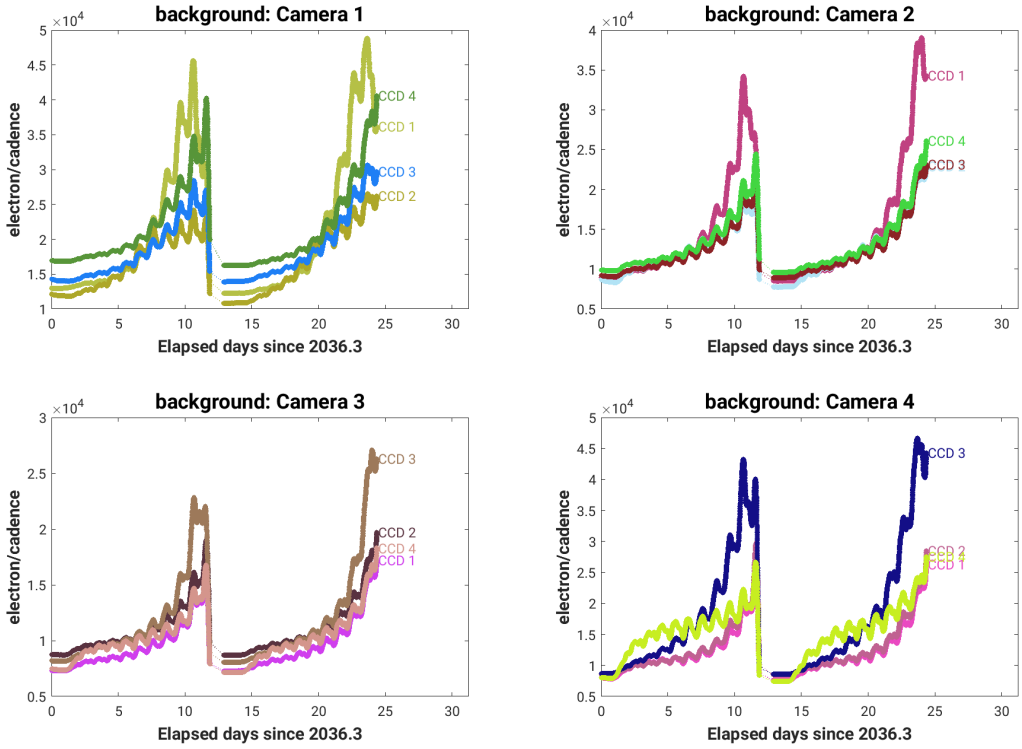

Figure 2: Median background flux across all targets on a given CCD in each camera. The changes are caused by variations in the orientation and distance of the Earth and Moon.

Cadences marked with bits 3, 4, 6, and 12 (Coarse Point, Earth Point, Reaction Wheel Desaturation Event, and Straylight) were marked based on spacecraft telemetry.

Cadences marked with bit 5 and 10 (Argabrightening Events and Impulsive Outlier) were identified by the SPOC pipeline. Bit 5 marks a sudden change in the background measurements. In practice, bit 5 flags are caused by rapidly changing glints and unstable pointing at times near momentum dumps. Bit 10 marks an outlier identified by PDC and omitted from the cotrending procedure.

The new 20-second data mode includes cadences marked with bit 7 and 11 (Cosmic Ray in Optimal Aperture and Cosmic Ray in Collateral Pixel). These flags indicate cadences affected by cosmic rays that are removed by the pipeline, and can be found in both the TPF and LC files. The data provided in the archive products are corrected for cosmic rays, and a `FITS` table extension in the TPF and Collateral Pixel File details the cosmic rays identified and removed by the pipeline at the pixel level. The cosmic ray mitigation algorithm implemented in the SPOC pipeline is described in §4.1.

Cadences marked with bit 8 (Manual Exclude) are ignored by PDC, TPS, and DV for cotrending and transit searches. In Sector 27, these cadences were identified using spacecraft telemetry from the fine pointing system. All cadences with pointing excursions >7 arcsec (0.3 pixel) were flagged for manual exclude. Figure 4 also shows an assessment of the performance of the cotrending based on the final set of manual excludes.

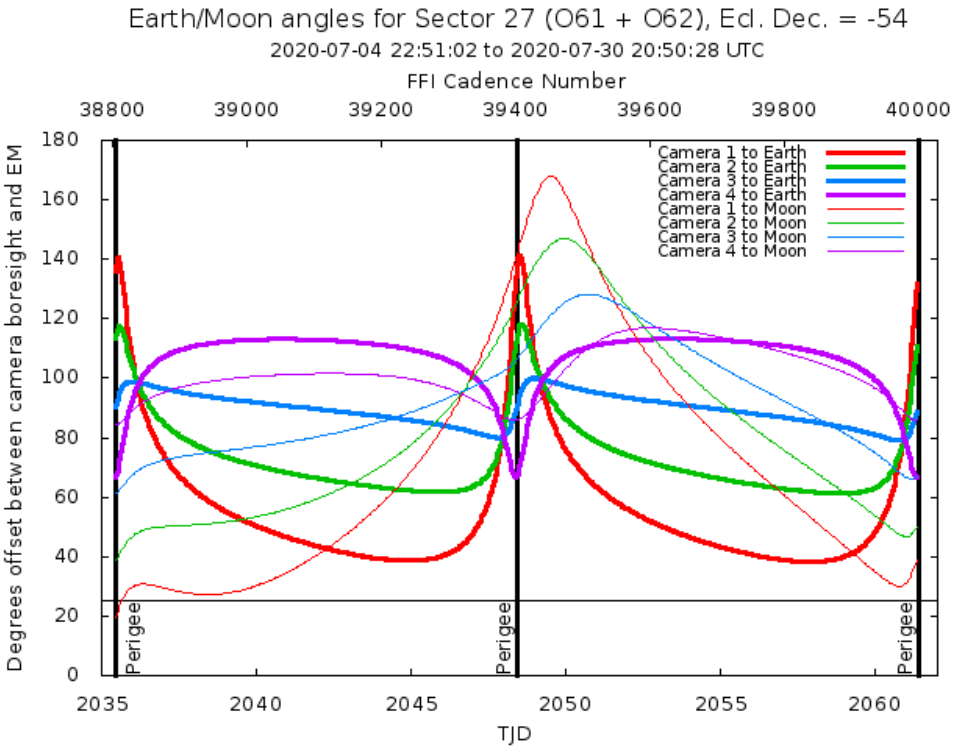

Figure 3: Angle between the four camera boresights and the Earth/Moon as a function of time. When the Earth is within $\sim 25°$ of a camera's boresight, transiting planet searches may be compromised by high levels of scattered light. At larger angles, up to $\sim 35°$, scattered light patterns and complicated structures may be visible. At yet larger angles, low level patchy features may be visible. Scattered light from the Moon is generally only noticeable below $\sim 35°$. This figure can be used to identify periods affected by scattered light and the relative contributions of the Earth and Moon to the background. However, the background intensity and locations of scattered light features depend on additional factors, such as the Earth/Moon azimuth and distance from the spacecraft.

In Sector 27, the predicted stray light flag (bit 12, value 2048) is disabled for the 2-minute and 20-second data products. Instead, the scattered light exclude flag (bit 13, value 4096) identifies cadences at which individual targets are affected by scattered light. The predicted stray light flag (bit 12) continues to be marked in the FFIs and flags times when the Earth/Moon are near the camera FOVs and may interfere with guiding or saturate the detectors. We strongly recommend that users inspect the FFI data before removing images marked with bit 12, because this bit is set based on predictions from mission planning and is known to be conservative with respect to the quality of data usable for analysis.

If the Earth/Moon interference is strong enough to saturate the detector, all targets on a CCD slice will be affected and the data are unusable. Cadences with bad calibrations due to saturation are now explicitly marked with bit 15 (value 16384, "Bad Calibration Exclude"). For some cadences, the majority of targets on a CCD may be flagged for scattered light and not enough valid data remains to derive cotrending basis vectors in PDC. No systematic error correction can be applied at these times. This situation is identified by bit 16 (value 32768, "Insufficient Targets for Error Correction Exclude").

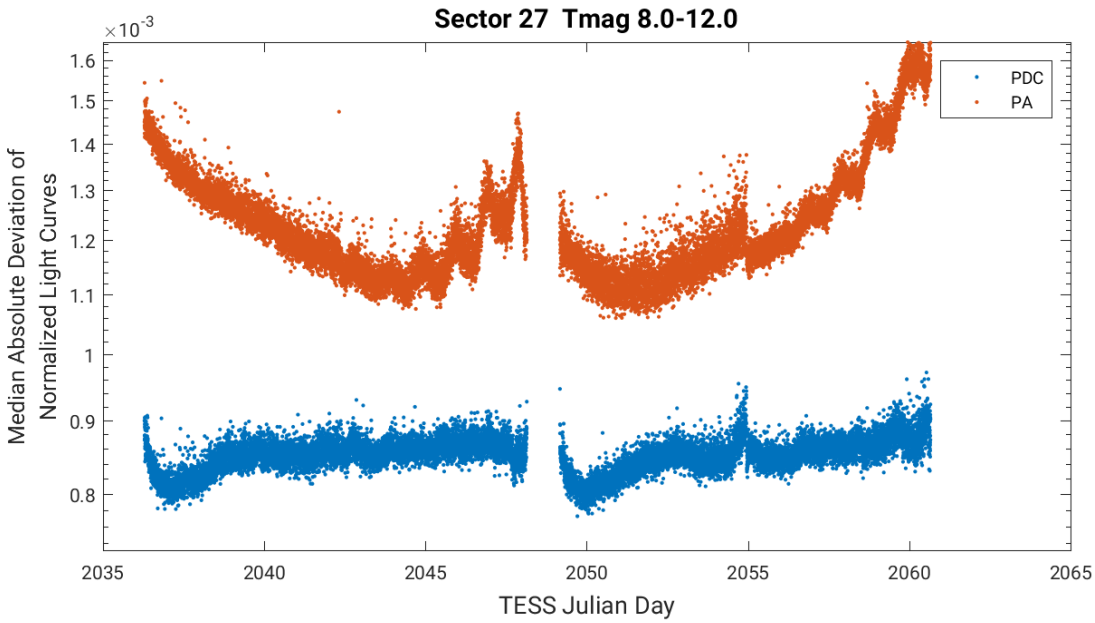

Figure 4: Median absolute deviation (MAD) for the two-minute cadence data from Sector 27, showing the performance of the cotrending after identifying Manual Exclude data quality flags. The MAD is calculated in each cadence across stars with flux variations less than 1% for both the PA (red) and PDC (blue) light curves, where each light curve is normalized by its median flux value. The scatter in the PA light curves is much higher than that for the PDC light curves, and the outliers in the PA light curves are largely absent from the PDC light curves due to the use of the anomaly flags.

FFIs were only marked with bits 3, 6 and 12 (Course Point, Reaction Wheel Desaturation Events and Straylight). Only one FFI is affected by each momentum dump. There are no WCS coordinates for FFIs that coincide with momentum dumps.

3 Anomalous Effects

3.1 Smear Correction Issues

The following columns were impacted by bright stars in the science frame, and/or upper buffer rows, and/or lower science frame rows, which bleed into the upper serial register resulting in an overestimated smear correction.

- Camera 4, CCD 1, Column 529, Star HD 30865
- Camera 4, CCD 1, Column 1060, Star WZ Doradus

3.2 Fireflies and Fireworks

Table 2 lists all firefly and fireworks events for Sector 27. These phenomena are small, spatially extended, comet-like features in the images—created by sunlit particles in the

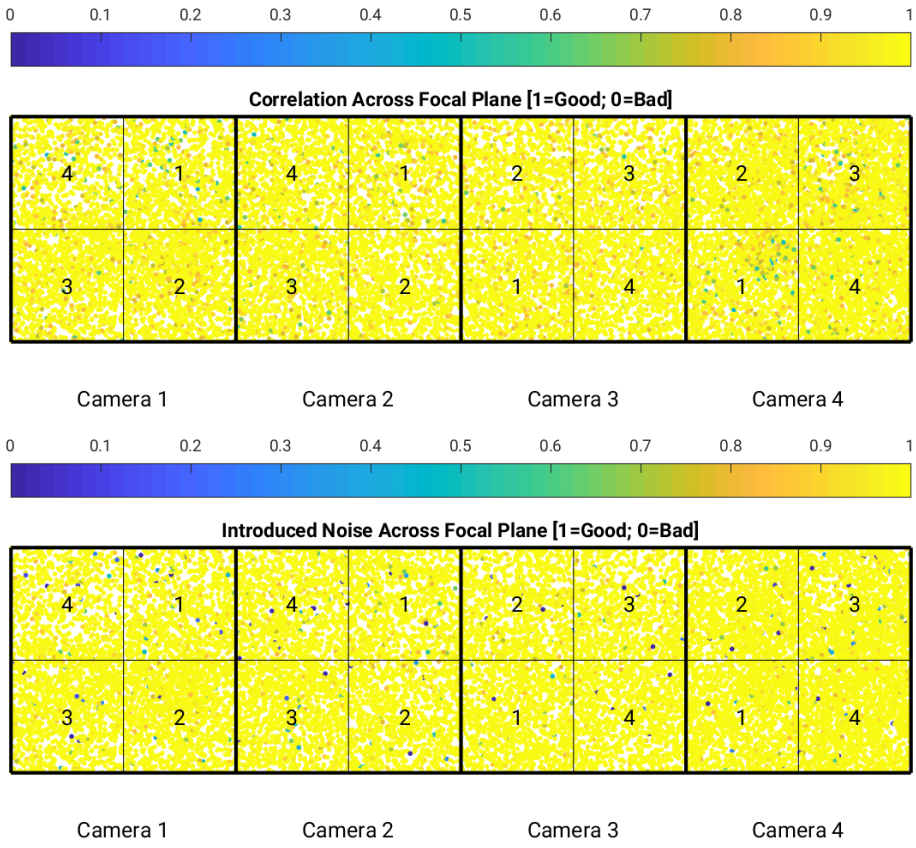

Figure 5: PDC residual correlation goodness metric (top panel) and PDC introduced noise goodness metric (bottom panel) for the two-minute cadence data. The metric values are shown on a focal plane map indicating the camera and CCD location of each target. The correlation goodness metric is calibrated such that a value greater than 0.8 means there is less than 10% mean absolute correlation between the target under study and all other targets on the CCD. The introduced noise metric is calibrated such that a value greater than 0.8 means the power in broad-band introduced noise is below the level of uncertainties in the flux values.

camera FOV—that may appear one or two at a time (fireflies) or in large groups (fireworks). See the TESS Instrument Handbook for a more complete description.

4 Pipeline Performance and Results

4.1 20-second Cadence Data Processing

Twenty-second cadence data were run through pipeline modules CAL, COA, PA, PDC, and TPS. These pipeline modules calibrate the pixels, compute optimal apertures, extract simple aperture photometry (`SAP_FLUX` light curves), remove common systematic errors with cotrending (`PDCSAP_FLUX` light curves), and calculate the combined differential photometric precision. The 20-second cadence data are not searched for transit signatures, so no Threshold Crossing Events (TCEs) or Data Validation products are produced. As discussed in §1.1

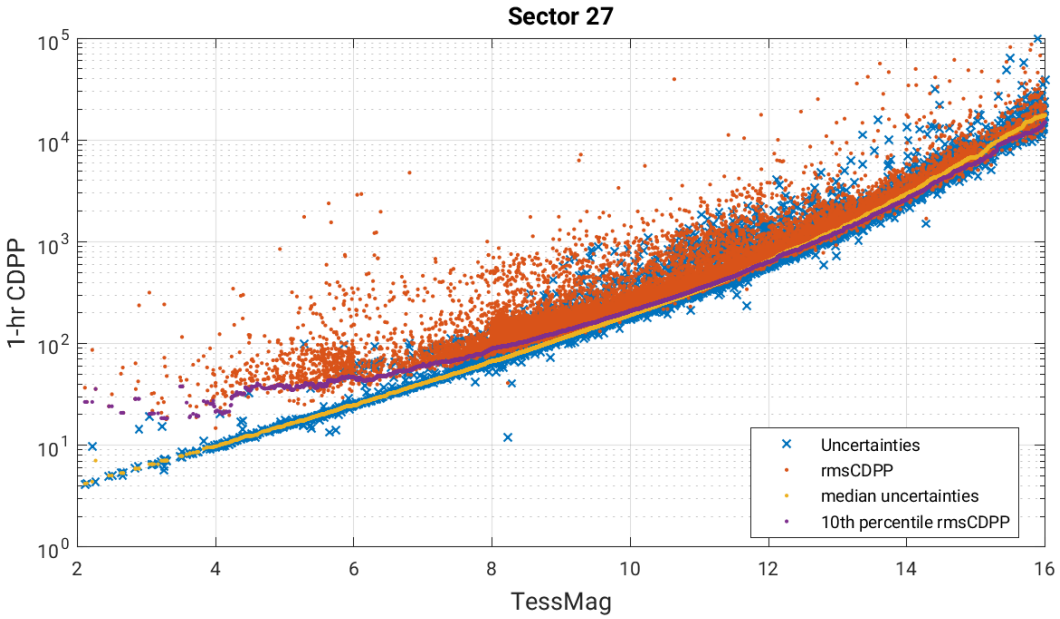

Figure 6: 1-hour CDPP. The red points are the RMS CDPP measurements for the 19,997 light curves from Sector 27 plotted as a function of TESS magnitude. The blue x's are the uncertainties, scaled to 1-hour timescale. The purple curve is a moving 10th percentile of the RMS CDPP measurements, and the gold curve is a moving median of the 1-hr uncertainties.

Table 2: Sector Fireflies and Fireworks

FFI Start	FFI End	Cameras	Description
2020192024916	2020192030916	2, 3	Fireflies
2020196130916	2020196131916	1	Firefly

earlier, all 20-second target stars are also observed at 2-minute cadence, and the 2-minute cadence light curves are searched for transits.

The CAL and PA modules also identify and correct cosmic ray hits in collateral and target pixels in the 20-second cadence data. The algorithm for cleaning cosmic rays in collateral pixels is based on that employed in the *Kepler* data processing pipeline, and is fully documented in Jenkins (2020, sec 6.3.1). The algorithm for cleaning cosmic rays in target pixels is new for TESS because of differences in the dominant systematic errors.

Cosmic rays are identified and corrected by PA in target pixel time series as follows. Pixel values for every cadence are predicted by a model based on delta-quaternions (Figure 1) and the measured background flux. After subtracting the model, the residual time series for each pixel is detrended with a moving median to remove long timescale stellar variations. Candidate cosmic ray hits are identified with an adaptive threshold based on noise estimates in a sliding window. For Sector 27 processing, the cosmic ray detection threshold was set to $5\,\sigma$ to limit the opportunity for triggering on astrophysical signatures such as flares. Estimates of the flux deposited by cosmic rays are obtained from the detrended residuals between the pixel time series and pixel model when the residuals exceed the detection threshold. Candi-

date cosmic ray detections in the photometric aperture are only accepted on cadences where (1) the aperture sum improves the smoothness of the flux time series (measured as the distance from each flagged data point to a local median), and (2) cosmic ray hits do not occur in the optimal aperture on three or more consecutive cadences; all candidate cosmic ray hits outside the photometric aperture are (currently) accepted.

Cosmic rays corrected by the pipeline are tabulated in a FITS extension in the 20-second cadence Target Pixel and Collateral Pixel Files. The tables give the cadence, CCD row, CCD column, and estimated charge deposited by the detected cosmic rays. Uncorrected pixel data can be reconstructed by adding the values in the `COSMIC_RAY` column of the TPF `TARGET COSMIC RAY` table to the appropriate pixel and cadence. The Data Anomaly Flags in the light curves identify cadences where cosmic ray hits were identified in the optimal aperture or collateral pixels that intersect the rows or columns of the optimal aperture. The SDPDD describes the format and layout of these tables.

The `SAP_FLUX` time series can be "uncorrected" by summing the values in the `COSMIC_RAY` table for all affected pixels in the optimal aperture at cadence n, and then adding this value, $\Delta f\,(n)$, to the `SAP_FLUX` value for cadence n. The `PDCSAP_FLUX` time series, $f_{\mathrm{PDCSAP\_FLUX}}\,(n)$, can be "uncorrected" by scaling $\Delta f\,(n)$ by the ratio of the crowding metric to the flux fraction correction and then adding this value to the `PDCSAP_FLUX` at cadence n:

$$f'_{\mathrm{PDCSAP\_FLUX}}\,(n) = f_{\mathrm{PDCSAP\_FLUX}}(n) + \Delta f(n)\frac{\mathrm{CROWDSAP}}{\mathrm{FLFRCSAP}}, \tag{1}$$

where $f'_{\mathrm{PDCSAP\_FLUX}}$ is the "uncorrected" `PDCSAP_FLUX`, and `CROWDSAP` and `FLFRCSAP` are the crowding metric and flux fraction correction reported in the LC and TPF files, respectively.

Some positive outliers due to uncorrected cosmic rays remain in the `SAP_FLUX` light curves produced in PA, particularly for relatively bright targets. These outliers are subsequently identified in PDC and flagged as "Impulsive Outliers"(data quality bit 10, value 512) in the TPF and light curve products. By masking cadences flagged with bit 10, most of these low amplitude cosmic rays will be removed from the light curves. However, users should inspect the data to determine if additional positive outliers are present that might be associated with cosmic rays.

Finally, the limited number of targets per CCD taken at 20-second cadence means that there are not always enough light curves to derive CBVs in PDC at the CCD level. Therefore, all 1,000 targets from the full TESS field-of-view are used to cotrend the 20-second cadence data.

4.2 Background Correction

The background correction employed in PA throughout the primary mission was updated for the extended mission. Relatively dim and/or crowded target stars were often subject to overestimated background levels, which would result in underestimated flux values and therefore overestimated transit depths. A procedure was added in Sector 27 processing to improve the accuracy of the background correction. This update applies to all 2-minute and 20-second targets. The change in the background estimates and relative transit depths is small ($< 2\%$ for transit depths and $< 1\%$ for planet radii) except for dim and/or crowded targets.

In the primary mission, the background level was estimated on each cadence by a trimmed mean of a set of background pixels selected around the periphery of each target. The background pixels are identified in the `APERTURE` extension of the TPF and LC files, and the background correction was applied on each cadence to all pixels in the target postage stamp. The background estimates and associated uncertainties are given in the `SAP_BKG` and `SAP_BKG_ERR` columns of the TPFs and light curves.

To mitigate against over-correction, the trimmed background estimates are reduced in Sector 27 by a scalar offset that forces the dimmest background-corrected pixels to values near zero. To account for noise, the third dimmest pixel in the postage stamp (averaged over time) is selected as a "bias pixel," subject to the following constraints: (1) the bias pixel is not included in the photometric aperture or a one-halo ring around it, (2) the bias pixel is not in close proximity to a saturated column, (3) the bias pixel does not fall on a bad CCD column, and (4) the bias pixel does not fall on a column with significant smear over-correction. The background correction is shifted so that the mean value of the "bias pixel" over time is zero. The "bias pixel" always starts at a negative value, and so this procedure always results in a decrease in the overall background correction. Note that some negative pixels are expected after background subtraction due to random fluctuations, which is why there is no requirement in the pipeline that the first or second dimmest pixels be positive or zero.

For TPFs from Year 1 and Year 2 that display significant negative pixels after background subtraction relative to the signal of interest, corrections for biases in the background can be applied with the following procedure. First, determine an estimate for the background bias, $bg_{\rm bias}$, from the offset of the background-corrected pixels used to determine the background correction and zero.[8] Next, scale $bg_{\rm bias}$ by the number of pixels in the optimal aperture, $N_{\rm optimal\,aperture}$, and then add this value to the `SAP_FLUX` time series. To adjust the `PDCSAP_FLUX`, scale $bg_{\rm bias}$ by both the number of pixels in the optimal aperture and the ratio of the crowding metric to the flux fraction correction, and then add this value to the `PDCSAP_FLUX`:

$$f''_{\rm PDCSAP\_FLUX}\,(n) = f_{\rm PDCSAP\_FLUX}(n) + bg_{\rm bias}\,N_{\rm optimal\ aperture}\frac{\rm CROWDSAP}{\rm FLFRCSAP}, \qquad (2)$$

where $f''_{\rm PDCSAP\_FLUX}$ is the background bias-adjusted `PDCSAP_FLUX`.

4.3 Updates to the Propagation of Uncertainties

A recent query by the user community led to the determination that the pixel level uncertainties have been overestimated since Sector 5, after the 2-D black model was updated. In previous sectors, uncertainties in the 2-D black model were propagated from CAL to the uncertainties on individual pixels. However, becauses the 2-D black is a static term, its uncertainty should not predict temporal scatter in the photometric measurements and has been eliminated from the error propagation in the pipeline. This issue primarily affected dim stars whose uncertainties were dominated by noise sources other than shot noise. For

[8]The `APERTURE` image extension in the LC and TPF files indicates which pixels were assigned to the background pixels and to the optimal aperture. See §6.2 of the SDPDD for more information.

data sets released before DR38, we recommend using empirical estimates of the scatter in the light curves rather than the reported uncertainties.

4.4 Light Curves and Photometric Precision

Figure 5 gives the PDC goodness metrics for the two-minute cadence data, with residual correlation goodness and introduced noise goodness shown on a scale between 0 (bad) and 1 (good). The performance of PDC is very good and generally uniform over most of the field of view. Figure 6 shows the achieved Combined Differential Photometric Precision (CDPP) at 1-hour timescales for all targets.

4.5 Transit Search and Data Validation

In Sector 27, the two-minute light curves of 19,997 targets were subjected to the transit search in TPS. Of these, Threshold Crossing Events (TCEs) at the 7.1 σ level were generated for 874 targets.

We employed an iterative method when conducting the Sector 27 transit search. The top panel of Figure 7 shows the number of TCEs at a given cadence that exhibit a transit signal from an initial run of TPS. The 3-σ peaks were used to define deemphasis weights for a second run of TPS, the results of which are shown in the bottom panel of Figure 7. The final set of TCEs and the results reported here are based on the second run of TPS. The values of the adopted deemphasis weights are provided in the DV timeseries data products for targets with TCEs.

The top panel of Figure 8 shows the distribution of orbital periods for the final set of TCEs found in Sector 27. The vertical histogram in the right panel of Figure 8 shows the distribution of transit depths derived from limb-darkened transiting planet model fits for TCEs. The model transit depths range down to the order of 100 ppm, but the bulk of the transit depths are considerably larger.

A search for additional TCEs in potential multiple planet systems was conducted in DV through calls to TPS. A total of 1185 TCEs were ultimately identified in the SPOC pipeline on 874 unique target stars. Table 3 provides a breakdown of the number of TCEs by target. Note that targets with large numbers of TCEs are likely to include false positives.

Note that for those targets observed both in Year 1 and Year 3, Year 3 processing was done using TIC 8.1, while TIC 7 was used for Year 1 processing, which may result in differences in results for certain targets. Reprocessing of Year 1 data with TIC 8.1 is underway at the SPOC, as of Fall 2020.

Table 3: Sector 27 TCE Numbers

Number of TCEs	Number of Targets	Total TCEs
1	628	628
2	194	388
3	44	132
4	4	16
5	3	15
6	1	6
–	874	1185

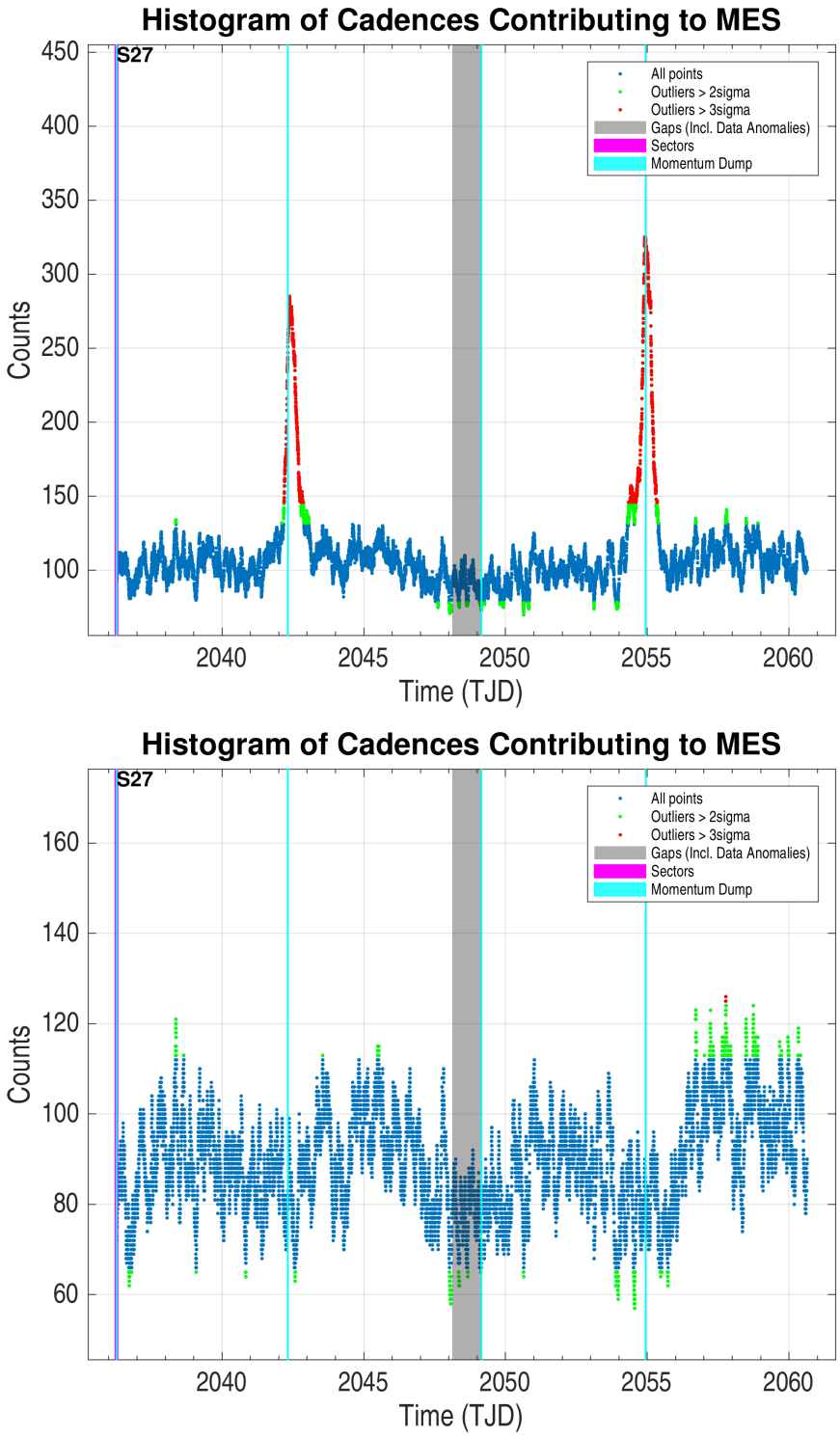

Figure 7: Top panel: Number of TCEs at a given cadence exhibiting a transit signal, based on an initial run of TPS. Any isolated peaks are caused by single events that result in spurious TCEs. These peaks were used to define deemphasis weights that suppress problematic epochs for the transit detection statistics in a second iteration of TPS. Bottom panel: Results from the second run of TPS.

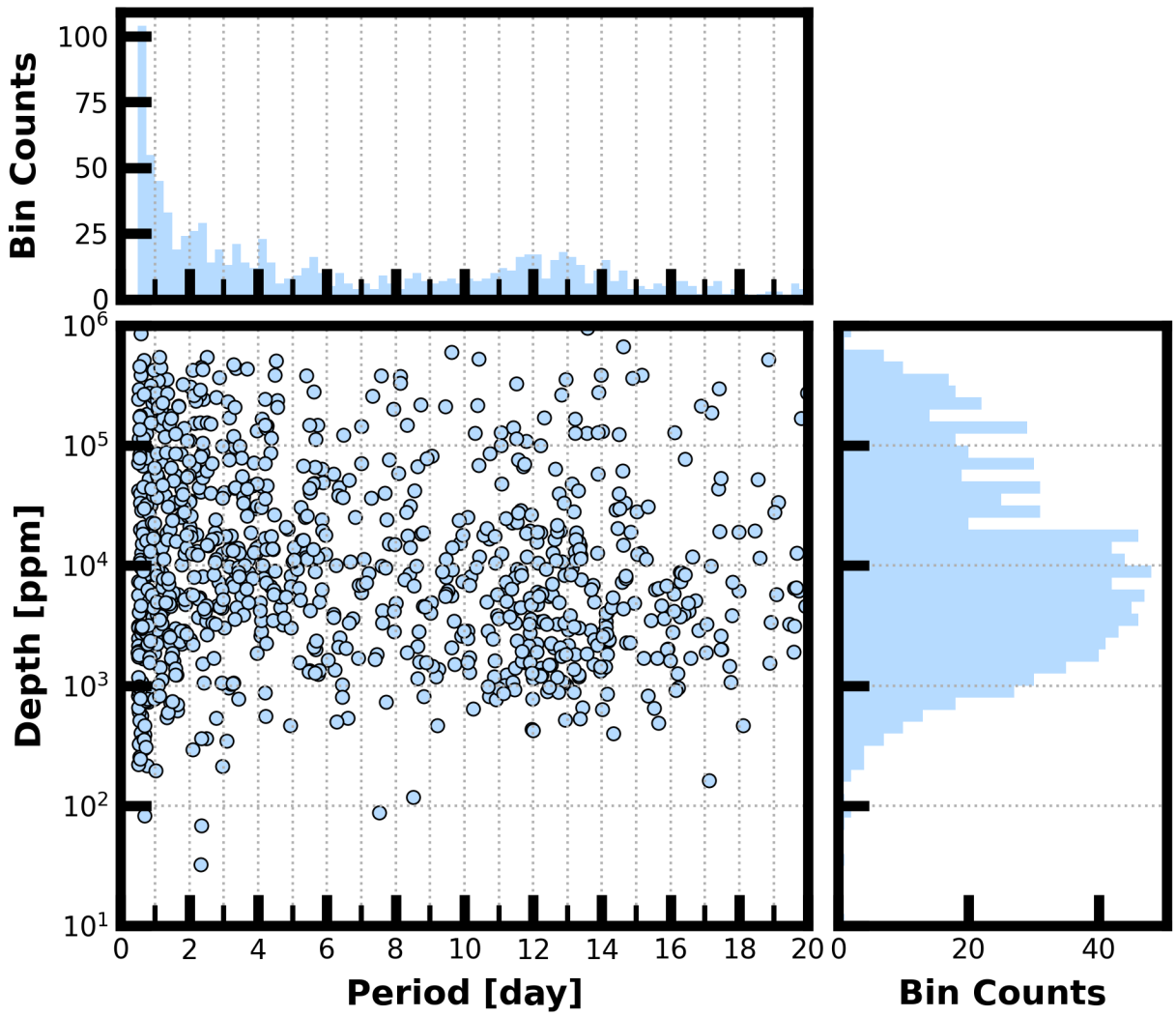

Figure 8: Lower Left Panel: Transit depth as a function of orbital period for the 1185 TCEs identified for the Sector 27 search. For enhanced visibility of long period detections, TCEs with orbital period <0.5 days are not shown. Reported depth comes from the DV limb-darkened transit fit depth when available, and the DV trapezoid model fit depth when not available. Top Panel: Orbital period distribution of the TCEs shown in the lower left panel. Right Panel: Transit depth distribution for the TCEs shown in the lower left panel.

References

Jenkins, J. M. 2020, Kepler Data Processing Handbook: Overview of the Science Operations Center, Tech. rep., NASA Ames Research Center

Jenkins, J. M., Twicken, J. D., McCauliff, S., et al. 2016, in Proc. SPIE, Vol. 9913, Software and Cyberinfrastructure for Astronomy IV, 99133E, doi: 10.1117/12.2233418

Li, J., Tenenbaum, P., Twicken, J. D., et al. 2019, *PASP*, 131, 024506, doi: 10.1088/1538-3873/aaf44d

Twicken, J. D., Catanzarite, J. H., Clarke, B. D., et al. 2018, *PASP*, 130, 064502, doi: 10.1088/1538-3873/aab694

Vanderspek, R., Doty, J., Fausnaugh, M., et al. 2018, TESS Instrument Handbook, Tech. rep., Kavli Institute for Astrophysics and Space Science, Massachusetts Institute of Technology

Acronyms and Abbreviation List

BTJD Barycentric-corrected TESS Julian Date

CAL Calibration Pipeline Module

CBV Cotrending Basis Vector

CCD Charge Coupled Device

CDPP Combined Differential Photometric Precision

COA Compute Optimal Aperture Pipeline Module

CSCI Computer Software Configuration Item

CTE Charge Transfer Efficiency

Dec Declination

DR Data Release

DV Data Validation Pipeline Module

DVA Differential Velocity Aberration

FFI Full Frame Image

FIN FFI Index Number

FITS Flexible Image Transport System

FOV Field of View

FPG Focal Plane Geometry model

KDPH Kepler Data Processing Handbook

KIH Kepler Instrument Handbook

KOI Kepler Object of Interest

MAD Median Absolute Deviation

MAP Maximum A Posteriori

MAST Mikulski Archive for Space Telescopes

MES Multiple Event Statistic

NAS NASA Advanced Supercomputing Division

PA Photometric Analysis Pipeline Module

PDC Pre-Search Data Conditioning Pipeline Module

PDC-MAP Pre-Search Data Conditioning Maximum A Posteriori algorithm

PDC-msMAP Pre-Search Data Conditioning Multiscale Maximum A Posteriori algorithm

PDF Portable Document Format

POC Payload Operations Center

POU Propagation of Uncertainties

ppm Parts-per-million

PRF Pixel Response Function

RA Right Ascension

RMS Root Mean Square

SAP Simple Aperture Photometry

SDPDD Science Data Products Description Document

SNR Signal-to-Noise Ratio

SPOC Science Processing Operations Center

SVD Singular Value Decomposition

TCE Threshold Crossing Event

TESS Transiting Exoplanet Survey Satellite

TIC TESS Input Catalog

TIH TESS Instrument Handbook

TJD TESS Julian Date

TOI TESS Object of Interest

TPS Transiting Planet Search Pipeline Module

UTC Coordinated Universal Time

WCS World Coordinate System

XML Extensible Markup Language